eXPRESS Polymer Letters Vol.11, No.5 (2017) 344–361
Available online at www.expresspolymlett.com
https://doi.org/10.3144/expresspolymlett.2017.34

UHMWPE/HDPE in-reactor blends, prepared by *in situ* polymerization: Synthetic aspects and characterization

A. E. Ferreira[1,2], M. L. Cerrada[3], E. Pérez[3], V. Lorenzo[4], E. Vallés[5], J. Ressia[5,6], H. Cramail[2], J. P. Lourenço[1,7], M. R. Ribeiro[1]*

[1]Centro de Química Estrutural, Instituto Superior Técnico – IST, Universidade de Lisboa, Portugal
[2]Laboratoire de Chimie des Polymères Organiques, UMR5629, Univ. Bordeaux, CNRS, INP-Bordeaux-ENSCBP, 16, Avenue Pey Berland, F-33607 Pessac Cedex, France
[3]Instituto de Ciencia y Tecnología de Polímeros (ICTP-CSIC). Juan de la Cierva 3, 28006 Madrid, Spain
[4]Grupo de Investigación 'POLímeros: Caracterización y Aplicaciones' (U. A. del ICTP-CSIC), E.T.S.I. Industriales, Universidad Politécnica de Madrid, José Gutiérrez Abascal 2, 28006 Madrid, Spain
[5]Planta Piloto de Ingeniería Química – PLAPIQUI (UNS-CONICET), Camino La Carrindanga Km 7, 8000 Bahía Blanca, Argentina
[6]Comisión de Investigaciones Científicas de la Provincia de Buenos Aires (CIC), La Plata, Argentina
[7]Faculdade de Ciências e Tecnologia - Universidade do Algarve. Campus de Gambelas, 8005-139 Faro, Portugal

Received 11 October 2016; accepted in revised form 19 December 2016

Abstract. This work covers the synthesis and characterization of in-reactor Ultra-High Molecular Weight Polyethylene/High Density Polyethylene, UHMWPE/HDPE, blends by *in situ* polymerization in a single reactor, through dual catalyst immobilization. These blends are synthesized combining two different catalysts (one for each targeted molar mass) co-immobilized in mesoporous Santa Barbara Amorphous, SBA-15, particles. First, the ethylene polymerization behavior is investigated, under different polymerization conditions. Then, studies on the thermal, mechanical and rheological characteristics of the produced in-reactor blends are presented and their performance is compared and discussed in a comprehensive way. Moreover, the effect of different filler contents on the properties exhibited by the resulting materials is investigated.
Results have shown that these in-reactor UHMWPE/HDPE blends exhibit a complex thermal, mechanical and rheological behavior, which depends mainly on the proportion between the two polymer components and on the amount of SBA-15.

Keywords: *polymer composites, in-reactor blends, UHMWPE*

1. Introduction

The widespread uses of ultra-high molecular weight polyethylene, UHMWPE, lead to the urgent development of approaches aiming to improve its performance. This is essential to fulfill its continuous market demands with tailored mechanical and/or thermal properties. Among these methods, the melt blending of UHMWPE with other polymers, different mineral particles, or addition of reinforcements [1–4] have proved to be an interesting strategy to attain these goals. Between polymers, high density polyethylene, HDPE, is a low price commodity, with good flow properties and feasible transformation by traditional processes, like extrusion, injection, blow molding, and rotational molding. Consequently, blends of UHMWPE and HDPE seem to be very interesting since the outstanding properties of UHMWPE and the good processability of HDPE under conventional techniques could be combined. Nevertheless, homogeneous HDPE/UHMWPE blends are rather difficult

*Corresponding author, e-mail: rosario@tecnico.ulisboa.pt

to be obtained by melt transformation processes because of mismatch of both, HDPE and UHMWPE, viscosities [5, 6].

Another methodology to combine UHMWPE and HDPE polymers into a unique material is by in-reactor blending using a multisite polymerization catalysts approach. This offers considerable cost and energy savings with respect to melt compounding since an intimate blending takes place during polymerization, which occurs at much lower temperatures and enables the mixing of immiscible components at a nanometer scale without requiring high shear forces.

Several studies from literature followed this route and have reported the use of homogeneous and supported multiple single-site catalysts, for the production of polyethylene with tailored molar mass distributions, MWDs, or branched polyethylene reactor blends in one reactor [7–10]. This approach has been also applied to the preparation of melt-processable HDPE/UHMWPE/blends with a high UHMWPE content. Namely, Mulhaupt reported on supported Fe/Cr dual- and triple-site catalysts that allow the easy control of the MWD of the polyethyelene, as a function of the Fe/Cr ratio and yield to UHMWPE/HDPE reactor blends [11–13]. In a recent review it is described the progress of multisite olefin polymerization catalysis and its impact on the preparation of advanced polyolefin materials and tailored reactor blends [14]. On the other hand, Rastogi and coworkers [15–18] explored a different and interesting alternative route to attain processable UHMWPE by lowering chain entanglement, through controlled synthesis conditions (low temperature, catalyst site isolation or favored crystallization over polymerization rate).

In this work these two approaches are combined in a new strategy, where the use of mixed single-site catalysts is coupled to the presence of a suitable support, SBA-15 mesoporous silica. The textural features of this ordered mesoporous support comprising nanometric pores allow the two catalysts to be anchored not only on the surface but also inside the ordered porous structure, leading to polyethylene chain growing inside the channels. Under this confined environment a more disentangled UHMWPE component may be formed. In addition, the role that mesoporous SBA-15 particles may play as fillers and how they will affect the mechanical performance of the issuing in-reactor blends constitutes another important aspect to be analyzed. It is expected that the combined strategy proposed here, may lead to high performance UHMWPE/HDPE polyethylene blends, reinforced by mesoporous silica, which may be easily processed as well.

The UHMWPE/HDPE polyethylene reactor blends will be prepared by *in situ* ethylene polymerization in a single reactor, using two different single-site catalysts (one for the synthesis of the UHMWPE component and the other one to obtain the corresponding HDPE). The proximity of different sites in a single catalytic support enables intimate blending of both polyethylene components on a nanometer-scale without requiring extensive shearing. In addition, the effect of the mesoporous SBA-15 particles as fillers constitutes other important aspect to be analyzed in these blends. The UHMWPE component is synthesized by a titanium bis-phenoxyimine complex (FI catalyst) while the polymerization of HDPE in the blend is carried out by the metallocene bis-(cyclopentadienyl) zirconium dichloride, Cp_2ZrCl_2, catalyst. The quasi-living behavior of FI catalyst allows a further degree of control for the tailoring of these blends since it affords an additional parameter, the polymerization time, for the tuning of its molar mass, M_W. The pre-activation (PA) method, which consists in the contact of both catalysts with methylaluminoxane, MAO, before their further interaction with the SBA-15 particles, has been selected as immobilization approach. Our previous results have shown that the diffusion of the catalyst within the support may be facilitated in the PA approach and that very high molar masses can be attained [19].

In this study UHMWPE/HDPE blends with different compositions, molar masses and filler contents (around 5 and 10 wt% of SBA-15) were prepared by varying the Ti:Zr molar proportion between the two single-site catalysts, the Al/M_T ratio (Al = aluminum; M_T = transition metal) and the polymerization time. The effect of these parameters on the polymerization activity is first analyzed. Then the influence of the blends molar mass and of the filler content on the properties exhibited by the resulting materials is discussed.

2. Experimental part

2.1. Materials and chemicals

All the chemicals for the synthesis of the SBA-15 particles: poly(ethyleneglycol)-*b*-poly(propyleneglycol)-*b*-poly(ethyleneglycol), P-123; hydrochloric acid (37% aq. sol.), tetraethylorthosilicate, TEOS; sodium chloride, NaCl; and ethanol, were purchased

from Sigma-Aldrich (St. Louis, USA) and used as received. All experiments for the SBA-15 modification and ethylene polymerization were carried out under dry nitrogen using standard Schlenk techniques. Ethylene and nitrogen (Air Liquide, Paris, France) were purified through absorption columns containing molecular sieves 4A and 13X. The bis [*N*-(3-*tert*-butylsalicylidene)-2,3,4,5,6-pentafluoroanilinate] titanium (IV) dichloride (FI catalyst, MCAT, Donaueschingen, Germany), bis-(cyclopentadienyl) zirconium dichloride (Zr catalyst, Sigma-Aldrich, St. Louis, USA) and methylaluminoxane (MAO, 7 wt% Al, AkzoNobel, Amsterdam, Netherland) were used as received. Toluene (VWR Chemicals, Radnor, USA) was dried by refluxing over metallic sodium under a dry nitrogen atmosphere, using benzophenone as indicator.

2.2. Preparation and characterization of pure SBA-15

The synthesis and characterization of pure SBA-15 was carried out as described elsewhere [19].

Briefly, 13.2 g of P-123 were first dissolved in 500 mL of water at room temperature, followed by the addition of 45 mL of 37% aq. sol. hydrochloric acid and 30.8 g of TEOS at 40 °C. After ca. 2 h, 12.3 g of NaCl were added and the final mixture was kept under stirring at 40 ºC for more 22 h. After an aging time of 3 days at 100 ºC the product was recovered by centrifugation, washed with distilled water until pH 6–7 and dried overnight at 80 °C. The template was partially removed by extraction with 96% ethanol, at reflux temperature for 16 h. The solid was further calcined under a flux of dry air at 550 °C for 12 h.

Prior to use, mesoporous SBA-15 particles were dried under a flux of dry air at 300 °C, for 1 h. Then, the support was kept at this temperature during another 1 h under a nitrogen flow and finally cooled down to room temperature and stored under dry nitrogen in a Schlenk flask.

SBA-15 was characterized by powder X-ray diffraction on a Panalytical X'Pert pro diffractometer using Cu K_α radiation filtered by Ni and a X'Celerator detector. The powder pattern (not shown) indicates the typical ordered hexagonal structure identified by the three diffraction peaks that can be indexed as (100), (110) and (200) associated with the *p6mm* hexagonal symmetry [19]. The textural properties were assessed by nitrogen adsorption at –196 ºC using an ASAP 2010 Micromeritics equipment. Prior to the measurement, the sample was degassed at 350 ºC for 3 h. The data show that this sample has a specific surface area of 758 m^2/g, a porous volume of 1.05 cm^3/g and an average porous diameter of 6.8 nm.

2.3. Ethylene polymerizations

Polymerizations were carried out in a 250 mL dried and nitrogen-flushed bottle for pressure reactions (Wilmad LabGlass LG-3921, Vineland, USA) magnetically stirred. The reactor was filled with 50 mL of toluene, and the adequate amounts of co-catalyst MAO, catalyst and ethylene. Polymerization took place at 20 °C and 1.1 bar of ethylene. Temperature, pressure and ethylene consumption were monitored in real time and the data stored, enabling acquisition of kinetic profiles. The polymerization was stopped by the addition of methanol acidified with 5% hydrochloric acid, HCl, when the intended amount of ethylene was consumed (allowing synthesizing nanocomposites with specific SBA-15 contents). Then the polymer was precipitated and washed twice with methanol before drying.

The synthesized polymer samples were named as follows: Zr and FI stands for the catalyst used, bis-(cyclopentadienyl) zirconium dichloride and bis [*N*-(3-*tert*-butylsalicylidene)-2,3,4,5,6-pentafluoroanilinate] titanium (IV) dichloride respectively, HOM for polymerizations carried out with an homogeneous catalyst, SBA for polymerizations performed with a supported catalyst and FIM is used for the blends prepared with the dual catalysts co-immobilized on SBA-15.

2.4. Preparation of the supported catalysts

The FI catalyst in toluene was pre-activated with MAO (Al/Ti = 150) by stirring it for 15 min at room temperature. Then, the equivalent of 0.85 μmol of MAO pre-activated catalyst was mixed with 100 mg of the support in toluene and stirred for 90 min. The total immobilization of FI catalyst on the support was confirmed by performing the clarified liquid test [20] and by elemental analysis of the supported catalyst.

2.5. Characterization of the polymers

High temperature size exclusion chromatography (HT-SEC) analyses were performed using a Viscotek system (Malvern Instruments, Malvern, UK) equipped with three columns (Polefin 300 mm×8 mm I. D. from Polymer Standards Service, porosity of 1000, 100 000 and 1000 000 Å). Sample solutions with

concentration of 5 mg·mL^{-1} were eluted in 1,2,4-trichlorobenzene using a flow rate of 1 mL·min^{-1} at 150 °C. The mobile phase was stabilized with 2,6-di(*tert*-butyl)-4-methylphenol. Online detection was performed with a differential refractive index detector and a dual light scattering detector for absolute molar mass measurement. The OmniSEC 5.02 software was used for calculations.

Polyethylene powders were processed as films by compression molding in a Collin P-200-P press (Ebersberg, Germany) between hot plates at 230 ºC for 2 min without pressure, 3 min at a pressure of 5 bar, then 2 min at 10 bar and finally cooling with cold water for 3 min at 10 bar.

Thermogravimetric analysis (TGA) was performed in a Q500 equipment of TA Instruments (New Castle, USA) under air or nitrogen atmosphere at a heating rate of 10 °C/min.

Calorimetric analyses were carried out in a TA Instruments (New Castle, USA) Q100 calorimeter connected to a cooling system and calibrated with different standards. The sample weights ranged from 3 to 5 mg. A temperature interval from –40 to 190 °C was studied at a heating rate of 10 °C/min. For the determination of the crystallinity, a value of 290 J/g was used as the enthalpy of fusion of a perfectly crystalline material [21].

TEM micrographs were obtained on a Hitachi H8100 equipment (Tokyo, Japan). Parallel cuts were prepared for the TEM analysis from different samples at –100 °C using a LEICA EM FC6 cryo-camera (Wetzlar, Germany) in order to attain thin sections (80 nm) of the film surface by means of the LEICA EM UC6 ultramicrotome (Wetzlar, Germany). Those cuts were picked up on cooper grids.

Depth Sensing Indentation, DSI, experiments were performed at room temperature with a Shimadzu tester (model DUH211S, Kyoto, Japan) equipped with a Berkovich type diamond indenter. At least 10 indentations were carried out at different regions of surface. The experimental protocol consisted in: a) the application of a load of 10 mN at a loading speed of 1.46 mN/s; b) the maintenance of this constant load for 5 s, and c) the release of the load at an unloading speed equal than the one used along the loading stage. Then, indentation depth was registered, additionally, for 5 s after reaching the minimum load (0.1 mN). Martens hardness, HMs, and indentation hardness, H_{it}, were calculated according to Oliver-Pharr method [22]. HMs is ascribed to elastic, viscoelastic and permanent strains, while H_{it} only depends on viscoelastic and plastic strains. Indentation modulus, E_{it}, was determined form the initial slope of the unloading curve.

The rheological characterization was carried out in a dynamic rotational rheometer, TA Instruments AR-G2 (New Castle, USA). To minimize polymer degradation the powder samples were previously treated with a solution of Irganox 1010 in acetone in an amount of Irganox equivalent to 1.5 wt% of the polymer and the experiments were carried under nitrogen atmosphere. Two equivalent linear rheological experiments, stress relaxation and oscillatory frequency sweep, were performed on some of the samples. The time-dependent relaxation modulus is obtained from the stress relaxation experiments, while the oscillatory frequency sweep allows the determination of the two frequency-dependent functions known as elastic, G', and viscous, G'', moduli. The time-dependent relaxation modulus is correlated via a Fourier transformation with the angular frequency tests to extend the dynamic data in the low frequency range. Both experiments were carried out using 25 mm diameter parallel plates at a temperature of 160 °C. The small-amplitude oscillatory shear mode measurements were carried out in a frequency range from 1 to 400 rad·s^{-1}. All tests were performed at small strains in order to assure the linearity of the dynamic responses [23]. To verify this, the series of frequency sweeps were repeated twice with the same sample at different strains, with excellent agreement.

3. Results and discussion

3.1. Ethylene polymerization behavior

The synthesis of the HDPE/UHMWPE blends was performed by varying the Ti:Zr molar proportion between the two single-site catalysts and the Al/M_T ratio. Furthermore, in order to investigate the effect of different filler contents on the properties exhibited by the resulting materials, a second set of polymerization runs was carried out under identical conditions but using a higher polymerization time. Thus, two sets of polyethylene blends, containing ~10 and 5 wt% of SBA-15 were synthesized. Due to the living nature of the FI catalyst [24–27], when changing the polymerization time, the effect of the different molar masses in the properties of the materials can also be evaluated.

The results obtained for the UHMWPE/HDPE blends together with the ones for the neat polymers and the

nanocomposites, prepared with each one of the two individual catalysts, are summarized in Table 1.

From these data it is clear that similarity was found in the activities at a given experimental condition, when synthesizing the blends with different SBA-15 (around 5 and 10%) contents. Figure 1 shows the kinetic profiles of two sets of polymerizations: FIM011 versus FIM012 and FIM004 versus FIM008 confirming the good reproducibility of data.

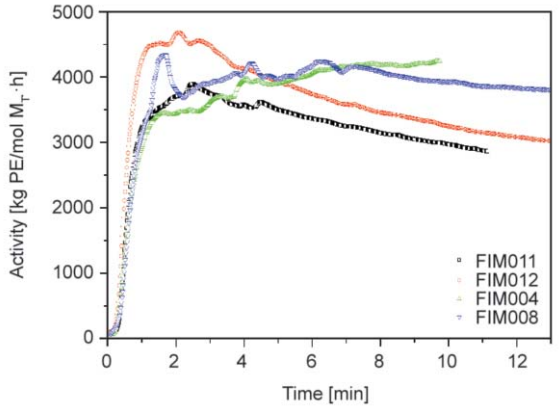

Figure 1. Kinetic profile for ethylene polymerizations. First set: FIM011 and FIM012; Second set: FIM004 and FIM008.

The activities values obtained during the preparation of the blends are in the range of the ones achieved for the individual supported catalysts used in the preparation of their respective ZrSBA009 or ZrSBA011 and FISBA016 or FISBA017 nanocomposites.

Table 1 also shows that, at a fixed Al/M_T ratio of 2500 and changing the Ti:Zr ratio from 20:80 to 80:20, the highest value of activity is obtained for the blend prepared with Ti:Zr of 50:50. This maximum on polymerization activity may be rationalized taking into account that, on one hand, the supported FI catalyst presents a higher activity than that reported for the supported zirconocene but, on the other hand, it also deactivates in a sharper and faster way, as clearly deduced from the different instantaneous activity profiles represented in Figure 2. Accordingly, an optimal polymerization activity is observed for conditions where those two opposing effects are balanced. Results on Table 1 also indicate that there is a trend of increasing activity for the blends prepared at a constant Ti:Zr molar proportion and increasing Al/M_T ratio.

As expected from literature, the molar masses of the polyethylenes obtained by the FI catalyst are much

Table 1. Polymerization conditions, activities, molar masses and dispersities, *D*, for the materials obtained with the bis [*N*-(3-*tert*-butylsalicylidene)-2,3,4,5,6-pentafluoroanilinate] titanium (IV), FI catalyst, and the metallocene, Cp_2ZrCl_2, both in homogeneous and supported conditions

Sample	Ti [mol%]	Zr [mol%]	Al/M_T	Reaction time [min]	Average activity [kg/molM_T·h]	SBA-15 [wt%]	M_w [g/mol]	*D*
Reference samples								
ZrHOM010	0	100	2500	5	14030	0	234000	3.0
ZrHOM008	0	100	1000	4	10260	0	–	–
ZrSBA009	0	100	2500	26	2540	9.6	200100	2.7
ZrSBA011	0	100	1300	20	1700	8.4	–	–
FIHOM002	100	0	2500	13	19310	0	1359000	1.5
FIHOM004	100	0	1500	13	19150	0	1479000	not data
FISBA016	100	0	1250	9	8122	6.9	1965000	1.9
FISBA017	100	0	2500	15	5460	8.5	838000	2.5
Blends								
FIM004	20	80	2500	10	3640	6.4	–	
FIM001	50	50	2500	7	4880	8.5	1066000	1.7
FIM005	80	20	2500	9	4040	12.5	990000	3.8
FIM011	50	50	500	11	3170	11.1	–	–
FIM006	50	50	1000	10	3450	10.8	1555000	3.5
FIM008	20	80	2500	19	3660	4.6	1270000	4.1
FIM013	50	50	2500	13	5430	4.3	1393000	1.8
FIM009	80	20	2500	17	4120	3.0	2162000	1.8
FIM012	50	50	500	21	3260	3.7	–	–
FIM010	50	50	1000	20	3500	3.6	1803000	3.4
FIM015 (H)*	50	50	2500	4	8443	0	410000	2.7

*FIM015 (H) is a blend synthesized under homogenous conditions, i.e., mesoporous SBA-15 particles have not been used as catalysts carrier.

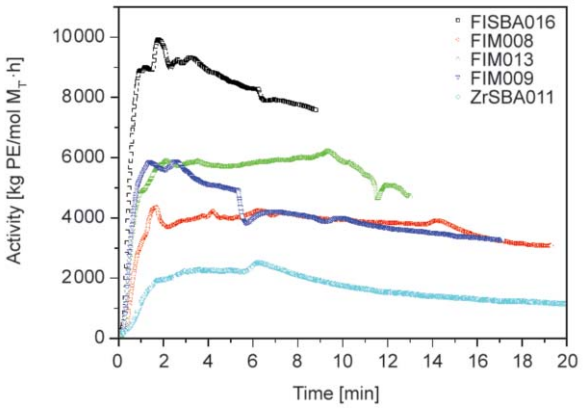

Figure 2. Kinetic profiles for ethylene polymerizations for the synthesis of two nanocomposites, FISBA016 and ZrSBA011 and three blends FIM008, FIM013 and FIM009

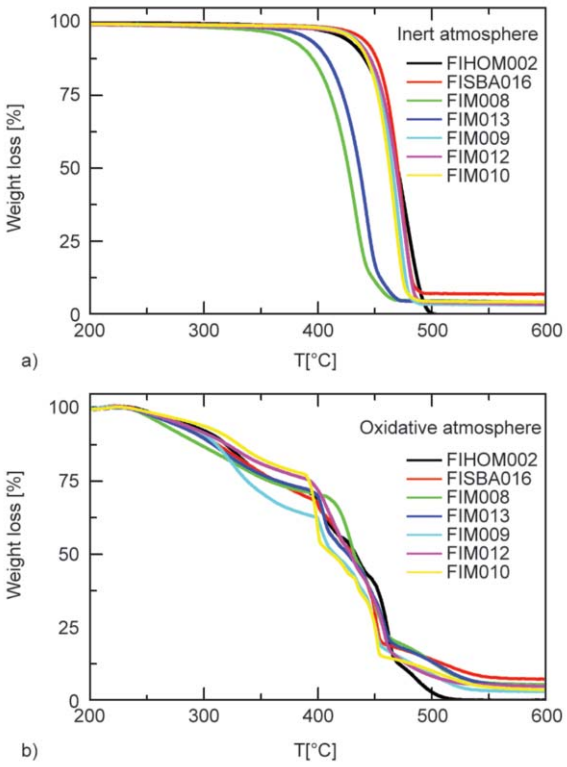

Figure 3. TGA curves of different UHMWPE/HDPE blends: at constant Al/M_T = 2500 and different (20:80, 50:50 and 80:20) Ti:Zr ratios (specimens FIM008, FIM013 and FIM009, respectively) as well as at 50:50 Ti:Zr proportion and distinct (500, 1000 and 2500) Al/M_T ratio (specimens under FIM012, FIM010 and FIM013, respectively), a) inert atmosphere and b) oxidative atmosphere

higher (about one order of magnitude) than the ones attained through the zirconocene catalyst (see Table 1). Accordingly, the molar masses of the blends, obtained at a fixed Al/M_T ratio for each set of polymerization runs, tend to increase with the molar proportion of the FI catalyst in the supported catalytic system. On the other hand, when fixing the Ti:Zr proportion at 50:50, the results seem to point out a decrease of the molar mass of the blends at increasing Al/M_T ratios (compare FIM010, and FIM013 or FIM001 and FIM006). This trend may be related to the role of trimethylaluminum, TMA (one of the different species present in MAO) on deactivation pathways that contribute to a loss of the polymerization control and that will reduce the polymer chain growth [19, 25].

3.2. Thermal properties

3.2.1. Thermogravimetric analysis

Figure 3 shows the thermogravimetric curves under inert and oxidative environments for the blends prepared at the longest times. The curves corresponding to the neat FI and a hybrid with SBA-15 have been also included for comparison. Looking at the upper plot, a single primary stage of decomposition is observed in the temperature range from 200 to 650 °C for all the specimens. On the contrary, four different degradation processes are noticeable at identical temperature interval when air is the atmosphere used, as depicted in the bottom plot of Figure 3.

A displacement to higher temperatures is observed for the degradation process under inert conditions as the FI relative content in the support is increased in the FIM008, FIM013 and FIM009 specimens synthesized at a constant Al/M_T ratio of 2500 (metal including Titanium and Zirconium that comes from both catalysts used). This feature might be ascribed to the differences found in the molar masses between the distinct samples, in such a way, that the blend becomes more stable and, consequently, its decomposition starts at higher temperature, as molar mass rises.

Thermal degradation of polyethylene has been reported to occur under inert environment through a random scission mechanism that turns out in the rupture of original polymeric chain [19, 28]. This degradation route is much simpler than the one under oxidative conditions and, consequently, four different processes are noticeable at an identical temperature interval when the TGA runs are performed in air.

The thermogravimetric curves obtained under oxidative atmosphere are depicted in the lower representation of Figure 3. They show that the effect of the distinct variables is more important up to a temperature around 400 °C. Above that temperature, the differences between specimens are rather less signifi-

Table 2. Average SBA-15 [wt% content], characteristic decomposition temperatures under nitrogen and air atmospheres for the UHMWPE/HDPE blends

Sample	Average SBA-15 [wt% content]	Inert atmosphere			Oxidative atmosphere		
		$T_{10\%}$ [°C]	$T_{25\%}$ [°C]	SBA-15 [wt%]	$T_{10\%}$ [°C]	$T_{25\%}$ [°C]	SBA-15 [wt%]
FIHOM002	0	437	455	0	311	364	0
FISBA016	6.9	448	461	6.8	302	363	7.0
FIM008	4.6	391	412	4.1	285	358	5.2
FIM013	4.3	403	422	4.0	299	366	4.5
FIM009	3.0	442	455	3.1	304	338	2.9
FIM012	3.7	443	458	3.1	309	393	4.3
FIM010	3.6	441	452	4.1	322	392	3.2

cant and the thermal response of the various blends is quite analogous. At a constant Al/M_T ratio of 2500 and varying the proportion of the catalyst supported in the mesoporous SBA-15, *i.e.*, FIM008, FIM013 and FIM009 specimens, $T_{10\%}$ dependence is similar to that found under inert conditions (see Table 2). Thus, a shift of the beginning of degradation process to higher temperatures is observed as FI content in SBA-15 is raised, this feature being ascribed to differences in molar masses of the blends. This trend changes at higher temperatures and the lowest $T_{25\%}$ value is now exhibited by FIM009, *i.e.*, the blend synthesized with the highest amount of FI.

Moreover, determination of the SBA-15 amount in the UHMWPE/HDPE blends is estimated from thermogravimetric analysis, TGA. Table 2 shows that the content for a given specimen is rather independent of the environment used. Average values obtained from inert and oxidative conditions are provided in Table 2. Figure 4 displays the effect on the thermal stability of increasing the amount of SBA-15 in different blends. Under inert conditions and at constant Al/M_T and Ti:Zr ratios it is clear that the presence of greater amount of SBA-15 leads to a significant displacement of the initiation of decomposition and its further progress. Therefore, SBA-15 particles seem to promote degradation. An analogous outcome is observed in oxidative atmosphere although the shift to lower temperatures is minimized. It appears that there is a merge of the two initial decomposition stages under these aggressive conditions, in the blends containing higher SBA-15 content.

This catalytic influence of the mesoporous materials in the degradation process of polyethylene has been already described in literature by Sinfronio *et al*. [29] and by Campos *et al*. [30]. Aguado *et al*. [31] have also shown the efficiency of mesoporous silica MCM-41 as promoter towards degradation of polyolefins into liquid fuels. Nowadays, this may be attractive in relation to the degradation of these polyolefins into basic petrochemicals as feedstock or fuel for downstream processes after their life service, making these self-reinforced polyolefinic materials environmentally welcome and with an added value [32].

3.2.2. Differential scanning calorimetry (DSC)

Figure 5 shows that the melting and crystallization processes appear as single peaks, indicating that both components undergo their phase transitions within identical temperature interval. This behavior could be expected taking into account that both present the same chemical structure and that blends have been prepared by *in situ* polymerization. Therefore, none conclusion on miscibility can be reached from DSC.

Looking first at the upper left melting processes (Figure 5a) related to the blends synthesized at a constant Al/M_T ratio of 2500 and varying the proportion of the catalysts supported in the mesoporous SBA-15, *i.e.*, FIM008, FIM013 and FIM009 specimens as well as FIM015 (which does not contain SBA-15) used for comparative reasons, a displacement of the main endothermic process to slightly higher temperatures is observed as Ti:Zr varies from 20:80 to 80:20 ratio. Then, the order of T_m increase is: FIM008 < FIM013 < FIM009, these values being highest that the one exhibited by the FIM015 blend synthesized with a 50Ti:50Zr ratio without SBA-15.

In addition to the shift of T_m by the presence of mesoporous particles, the appearance of a small shoulder in the temperature interval ranging from 100 to 125 °C is noticeable in the blends with SBA-15. This secondary process is less intense in sample FIM009 since its SBA-15 content is the lowest one. This small endothermic peak is attributed to those polyethylene crystallites, either those coming from the UHMWPE or from the HDPE component, that are

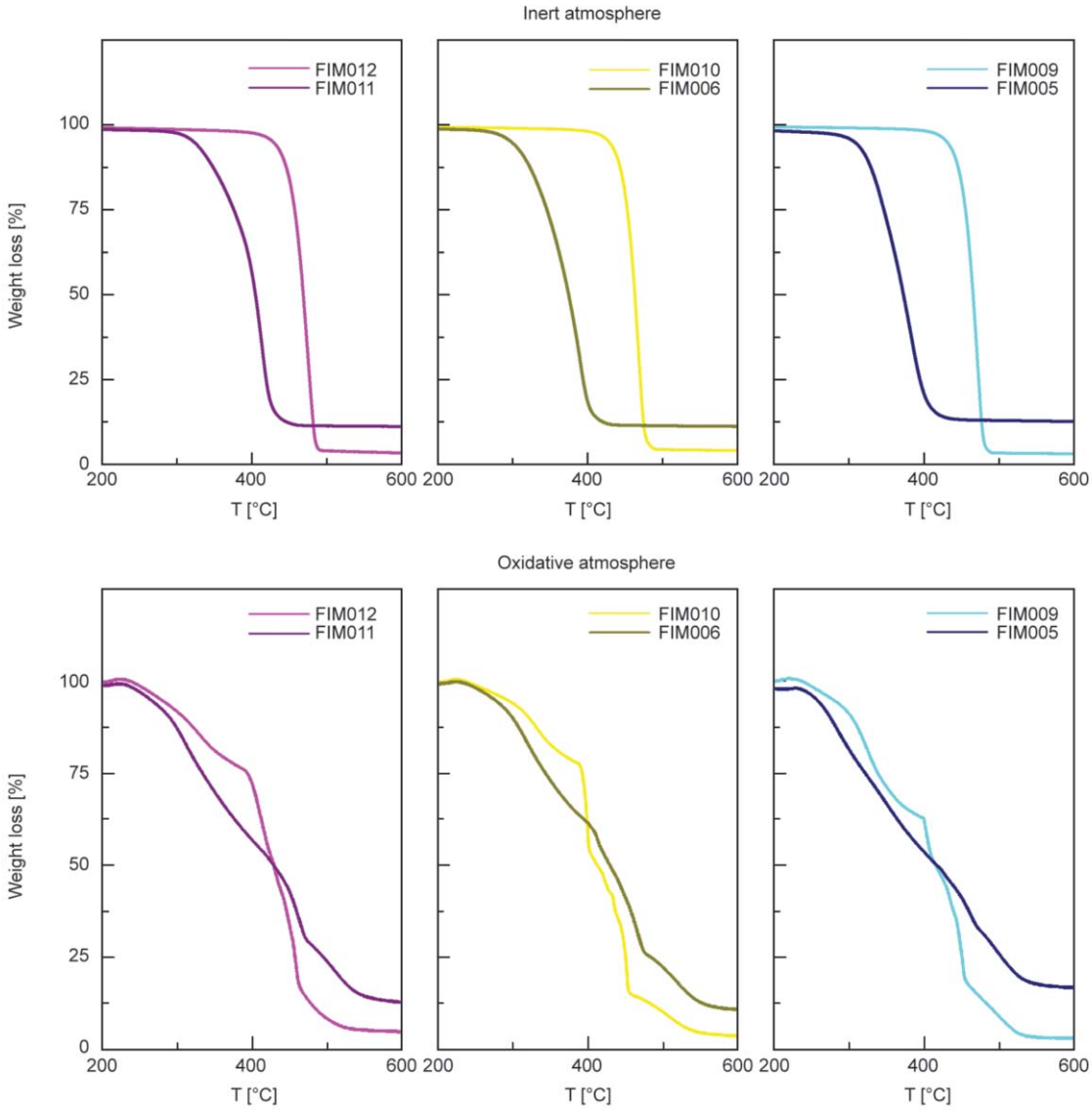

Figure 4. TGA curves of different UHMWPE/HDPE blends at constant Ti:Zr proportion and distinct (500, 1000 and 2500) Al/M_T ratios varying the content in SBA-15

developed inside the SBA-15 channels [19], similarly to evidence found in nanocomposites with MCM-41 [33, 34]. Channel confinement prevents a further growth of the crystallites and, accordingly, these crystalline entities generated within SBA-15 particles are of much smaller size than those that can grow at its surface and in the UHMWPE and HDPE bulks.

Concerning their further crystallization, there is not significant variation in the location of T_c for these samples, as deduced from data reported in Table 3 and from Figure 5b.

Figures 5c and 5d represent the features found in the blends containing a higher amount in SBA-15 particles at the identical 50:50 Ti:Zr ratio and different Al/M_T proportions. The T_m's are similar for these three samples (FIM011, FIM006 and FIM001) and higher than the observed one in the blend without SBA-15 (FIM015 sample) similar to what is observed in the blends with less mesoporous particles. Nevertheless, crystallinity is now increased for the samples with the highest SBA-15 content, as listed in Table 3. No evident nucleating effects are observed during crystallization at those high SBA-15 contents. On the other hand, the blends at a constant Al/M_T of 2500 do not show a clear trend for the values of crystallinity obtained from the first melting process. In what concerns the crystallization, there is a considerable difference in the degree of crystallinity (FIM004 > FIM001 > FIM005) developed during this process and the variation might be related to the increasing content in SBA-15. It has been reported [24] for HDPE nanocomposites reinforced with MCM-41

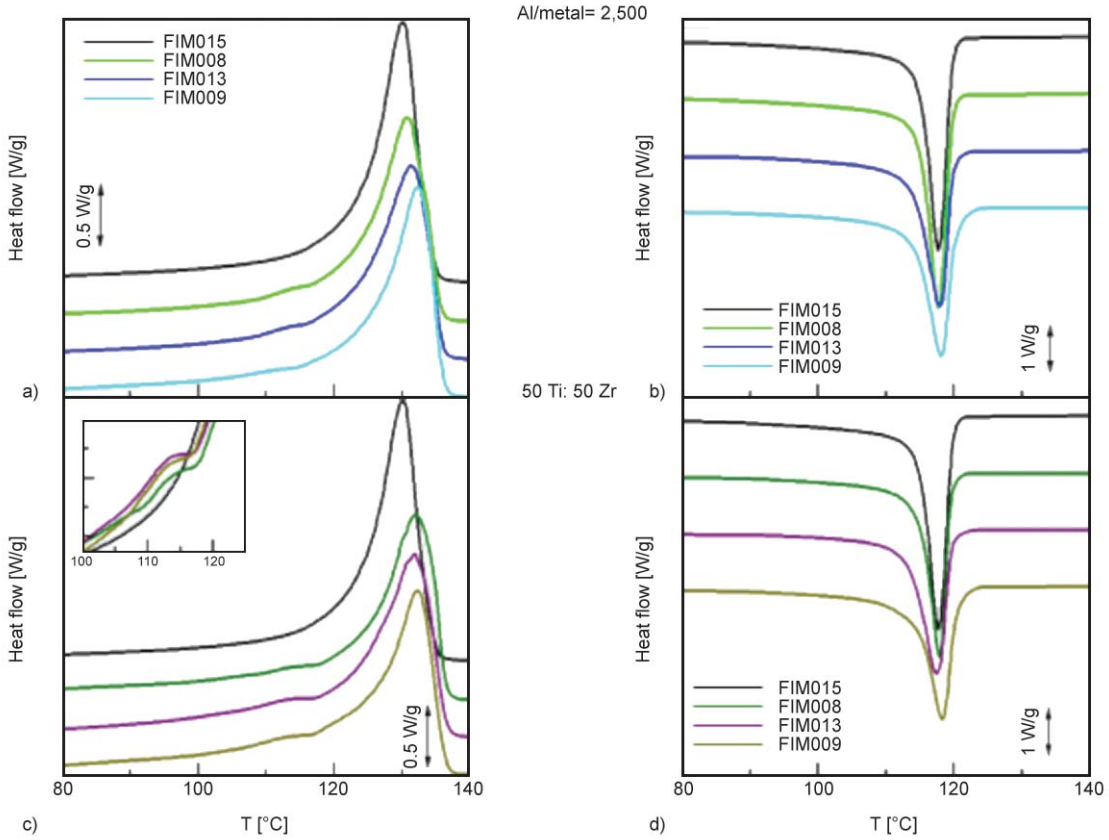

Figure 5. DSC curves of the first melting (plots, a) and c)) and subsequent crystallization processes (plots, b) and d)) of the blend without SBA-15 (FIM015) and on the top: blends with the lowest SBA-15 content at Al/M_T = 2500 and different Ti:Zr ratios: FIM008 (20:80), FIM013 (50:50) and FIM009 (80:20). On the bottom: blends with highest SBA-15 content at 50:50 Ti:Zr proportion and distinct Al/MT ratio: FIM001 (500), FIM011 (1000) and FIM006 (2500). The melting region of the small crystallites is represented in inset of c) plot.

Table 3. DSC calorimetric data of the materials prepared

Sample	Ti [mol%]	Zr [mol%]	SBA-15 [wt%]	M_w [g/mol]	f_c^m	T_m	f_c^c	T_c
ZrHOM010	0	100	0.0	234000	0.58	129.5	0.60	118.0
FIHOM002	100	0	0.0	1359000	0.53	131.0	0.54	118.0
FISBA016	100	–	6.9	1965000	0.49	132.5	0.47	118.0
FIM004	20	80	6.4	–	0.52	130.5	0.52	118.5
FIM001	50	50	8.5	1066000	0.52	132.0	0.49	118.0
FIM005	80	20	12.5	990000	0.55	132.0	0.43	117.5
FIM011	50	50	11.7	–	0.55	132.0	0.47	117.5
FIM006	50	50	10.8	1550000	0.54	132.5	0.47	118.5
FIM008	20	80	4.6	1270000	0.48	130.5	0.48	118.5
FIM013	50	50	4.3	1393000	0.48	131.0	0.49	118.0
FIM009	80	20	3.0	216200	0.48	132.5	0.47	118.0
FIM012	50	50	3.7	–	0.52	132.0	0.49	118.0
FIM010	50	50	3.6	1803000	0.49	132.0	0.49	118.0
FIM015 (H)	50	50	–	410000	0.49	130.0	0.51	118.0

f_c^m crystallinity for first melting and f_c^c crystallinity for crystallization

that crystallization process is delayed at contents of MCM-41 around 10 wt%. This was associated with the slower development of those crystallites belonging to chains within channels, *i.e.*, generated under great constraints. Then, confinement of the UHMWPE and HDPE matrices makes that crystallization within the channels requires much more time than the one involved in the DSC experiment. If the blends are allowed remaining enough time at room temperature (hours), crystallization of all the constrained polymer

chains is accomplished independently of their molar masses, and the number of crystal entities increases up to attain similar crystallinity than that achieved during first melting process.

3.3. Mechanical behavior

Indentation measurements have been chosen to evaluate preliminary the mechanical response of the UHMWPE/HDPE blends. Data from these experiments, concerning the elastic modulus and hardness, E_{it} and H_{it}, respectively, are detailed in Table 4 for the specimens with high SBA-15 contents. The pristine polyethylenes prepared from homogeneous zirconocene and FI catalysts, ZrHOM010 and FIHOM002, respectively, as well as their hybrids with SBA-15, ZrSBA011 and FISBA016, respectively, are examined before analyzing the UHMWPE / HDPE based blends.

Table 4 indicates that the samples synthesized using zirconocene catalyst either under homogeneous (ZrHOM010) or supported (ZrSBA011) conditions exhibit higher E_{it} and H_{it} values than those materials prepared by the FI catalyst (FIHOM002 and FISBA016, respectively). This fact is correlated to the deformation mode applied during the experiment since crystallinity is a key parameter in rigidity. HDPE usually shows a degree of crystallinity higher than the one developed in UHMWPE because of the large length of its macrochains [35]. Differences are reduced if the respective nanocomposites are compared (ZrSBA011 and FISBA016 samples), *i.e.*, when rigid SBA-15 particles, playing the dual role of support and filler, are incorporated. This behavior may be related to the fact that the reinforcement effect of SBA-15 is stronger and, accordingly, more noticeable when these particles are introduced on a less crystalline and softer UHMWPE matrix than when incorporated into an already more crystalline and harder HDPE polymer.

Additional variations are also clearly observed from regular representations of indentation experiments. Figure 6a shows that the largest depth reached after applying identical force load corresponds to the neat polyethylene synthesized using the FI catalyst. This feature indicates that sample FIHOM002 is the softest material and, then, indenter can penetrate deeper inside its surface. Moreover, its depth dependence on time, directly related to its deformability, is the greatest one, as depicted in Figure 6b, when the response is compared with that exhibited by the ZrHOM010 pristine polyethylene and the FIM015 blend, *i.e.* a UHMWPE / HDPE reactor blend prepared with a 50:50 Ti:Zr molar proportion without adding SBA-15 particles.

The effect of SBA-15 incorporation in HDPE and UHMWPE matrices is discussed below. The ZrSBA011 sample containing around 10 wt% in SBA-15 exhibited E_{it} and H_{it} values of 950 and 65 MPa, respectively. E_{it} does not practically change when compared to the corresponding neat HDPE but a significant increase in hardness is observed for the hybrid material. This fact seems to indicate that at those contents the presence of SBA-15 mainly affects the mechanical properties at the surface. Nevertheless, SBA-15 changes either bulk rigidity or superficial hardness in the softer materials, *i.e.*, those materials synthesized with the FI catalyst. Then, differences found in both parameters are considerable,

Table 4. Indentation parameters attained at 25 °C: indentation modulus (E_{it}) and hardness (H_{it}) for some pristine polyethylenes and nanocomposites as well as for the reactor blends prepared under different experimental conditions

Sample	Ti [mol%]	Zr [mol%]	SBA-15 [wt%]	M_w [g/mol]	f_c^{DSC}	H_{it} [MPa]	E_{it} [MPa]
ZrHOM010	0	100	0.0	234 000	0.66	53	985
ZrSBA011	0	100	10.9	–	0.63	65	950
FIHOM002	100	0	0.0	1359 000	0.53	44	684
FISBA016	100	–	6.9	1965 000	0.49	60	865
Blends							
FIM004	20	80	6.4	–	0.52	68	1093
FIM001	50	50	8.5	1066 000	0.52	65	973
FIM005	80	20	12.5	990 000	0.55	63	831
FIM011	50	50	11.7	–	0.55	65	961
FIM006	50	50	10.8	1555 000	0.54	70	1009
FIM015 (H)	50	50	–	410 000	0.49	55	893

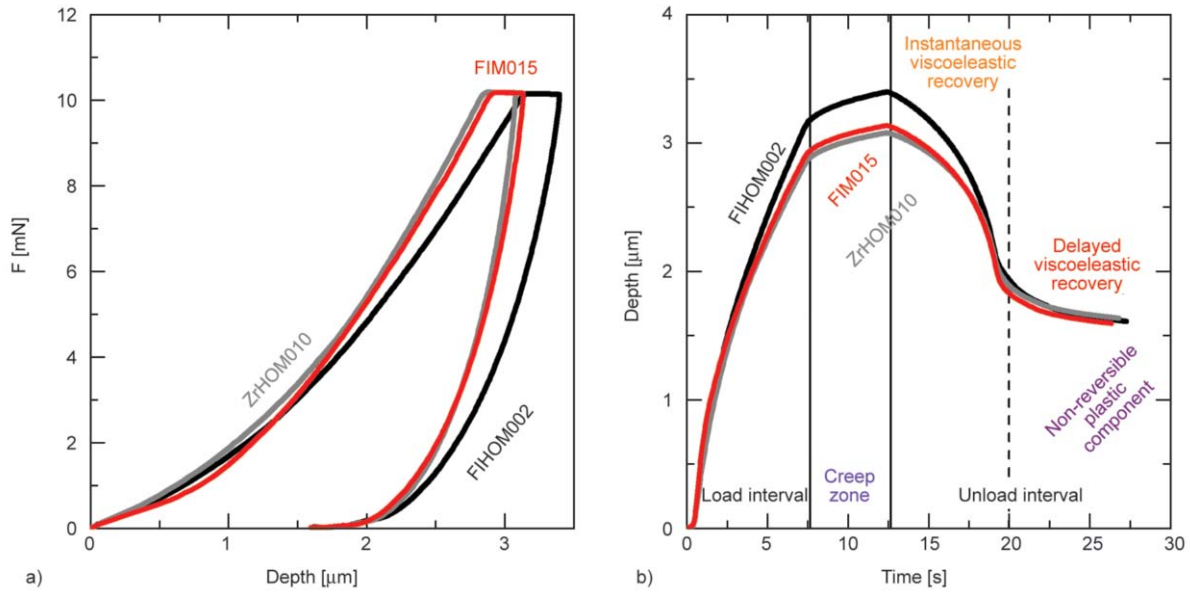

Figure 6. a) Indentation curves of load-maintenance-unload vs. depth for FIHOM002 and ZrHOM010 neat polymers and the FIM015 blend (50:50 Ti:Zr); b) Indenter depth dependence on experimental time

and the E_{it} increases from 684 MPa in FIHOM002 specimen to 865 MPa in the FISBA016 sample and H_{it} from 44 to 60 MPa, respectively.

Figure 7 shows the reinforcement role that SBA-15 particles exert in a UHMWPE/HDPE blend containing 8.5 wt% of SBA-15 (FIM001), prepared at identical synthetic conditions to those used for the neat FIM015 blend. Then, on one hand, indenter depth after applying identical force is inferior in the FIM001 sample and, on the other hand, the FIM001 blend containing the mesoporous SBA-15 shows a higher rigidity and hardness (see Table 4). It has been reported that these mechanical parameters only undergo significant enhancements in HDPE synthesized with zirconocene [33, 36] immobilized onto MCM-41 at filler loads ~30% and HDPE prepared with Hafnium catalyst supported on SBA-15 at filler contents >8 wt%.

The UHMWPE/HDPE blends exhibit a behavior dependent on the Ti:Zr ratio used during polymerization. E_{it} and H_{it} values increase as Zr amount is raised in the Ti:Zr molar proportion (see Table 4). Figure 8 displays also the soft character and easy deformability of the FIHOM002 neat polymer in comparison

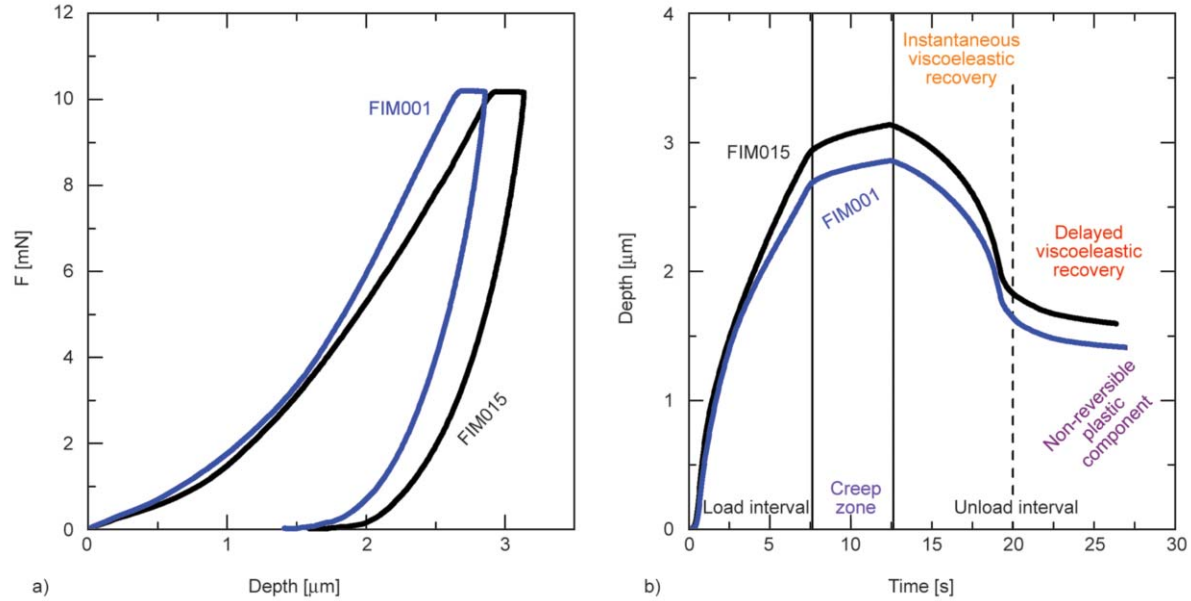

Figure 7. a) Indentation curves of load-maintenance-unload vs. depth for the neat FIM015 ($Al/M_T = 2500$) and the FIM001 (50:50 Ti:Zr, $Al/M_T = 2500$) blends. b) Indenter depth dependence on experimental time

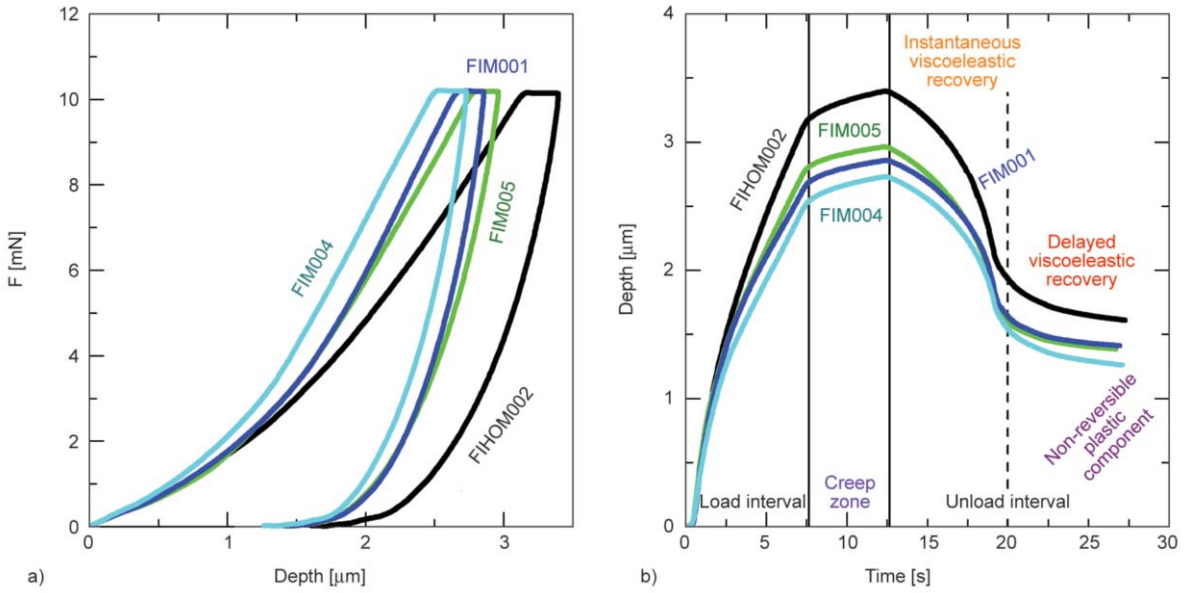

Figure 8. a) Indentation curves of load-maintenance-unload vs. depth for FIHOM002 and the blends synthesized at Al/M_T = 2500 and different Ti:Zr ratios: (80:20) FIM005; (50:50) FIM001; and, (20:80) FIM004. b) Indenter depth dependence on experimental time

with the FIM004 blend that contain a major amount of HDPE synthesized from the zirconocene catalyst. FIM001 and FIM005 blends are in between because of their different contents in UHMWPE and HDPE. Table 4 shows that the primary variable in these blends is their HDPE content, this parameter being even more important than the SBA-15 amount existing in the composite. Then, a reduction in rigidity and hardness values is observed as UHMWPE amount is expected to increase in the blend, *i.e.* as Ti:Zr molar proportion is raised.

A reinforcing effect might be also noticed by the addition of a minor UHMWPE amount to a HDPE matrix (samples FIM004 and ZrSBA011 in Table 4). Despite the smaller SBA-15 content and the lower crystallinity of the blend (obtained from a Ti:Zr molar proportion of 20:80) when compared to the HDPE composite sample (synthesized from a 0:100 Ti:Zr molar proportion) an increase of the E_{it} up to ~1100 MPa is observed for the blend. On the other hand when comparing the sample FISBA016 (prepared with a Ti:Zr molar proportion of 100:0) with the blend FIM005 (prepared from a Ti:Zr molar proportion of 80:20), no increase of modulus is observed, despite the higher crystallinity and SBA-15 content in the latter sample. Therefore, no reinforcement effect is observed upon addition of a small amount of a HDPE component to a UHMWPE matrix.

Table 4 also shows that there is not a clear trend as the Al/M_T ratio is changed at constant 50:50 Ti:Zr proportion. Then, E_{it} and H_{it} values are rather analogous.

It is well known that size and dispersion state of the filler affects mechanical properties of the composites. Figure 9 shows TEM micrographs for FIM004 and FIM005 samples, containing 6.4 and 12.5 wt% of SBA-15, respectively.

Changes found in SBA-15 dispersion are not very significant. The FIM005 sample seems, however, to present worse dispersed particles and aggregates of larger sizes, which may contribute to its lower mechanical performance. Interestingly, the SBA-15 channel like structure is clearly seen on the highest magnification pictures, confirming that the mesoporous structure has been neither altered nor lost after polymerization.

Creep characteristics can be deduced from the stage at constant force (F = 10 mN) in these indentation experiments. Three main parameters are important to explain the behavior of UHMWPE/HDPE blends under study: overall crystallinity, average molar mass since entanglements might play a considerable role to avoid creep and SBA-15 content because of its rigidity.

Figure 10 shows the variation in depth for the blends without and with SBA-15 at different Ti:Zr molar proportion and at constant Al/M_T ratio.

FIM015 blend prepared under homogeneous conditions is a rather soft material (E_{it} and H_{it} are quite small). This characteristic together with its low

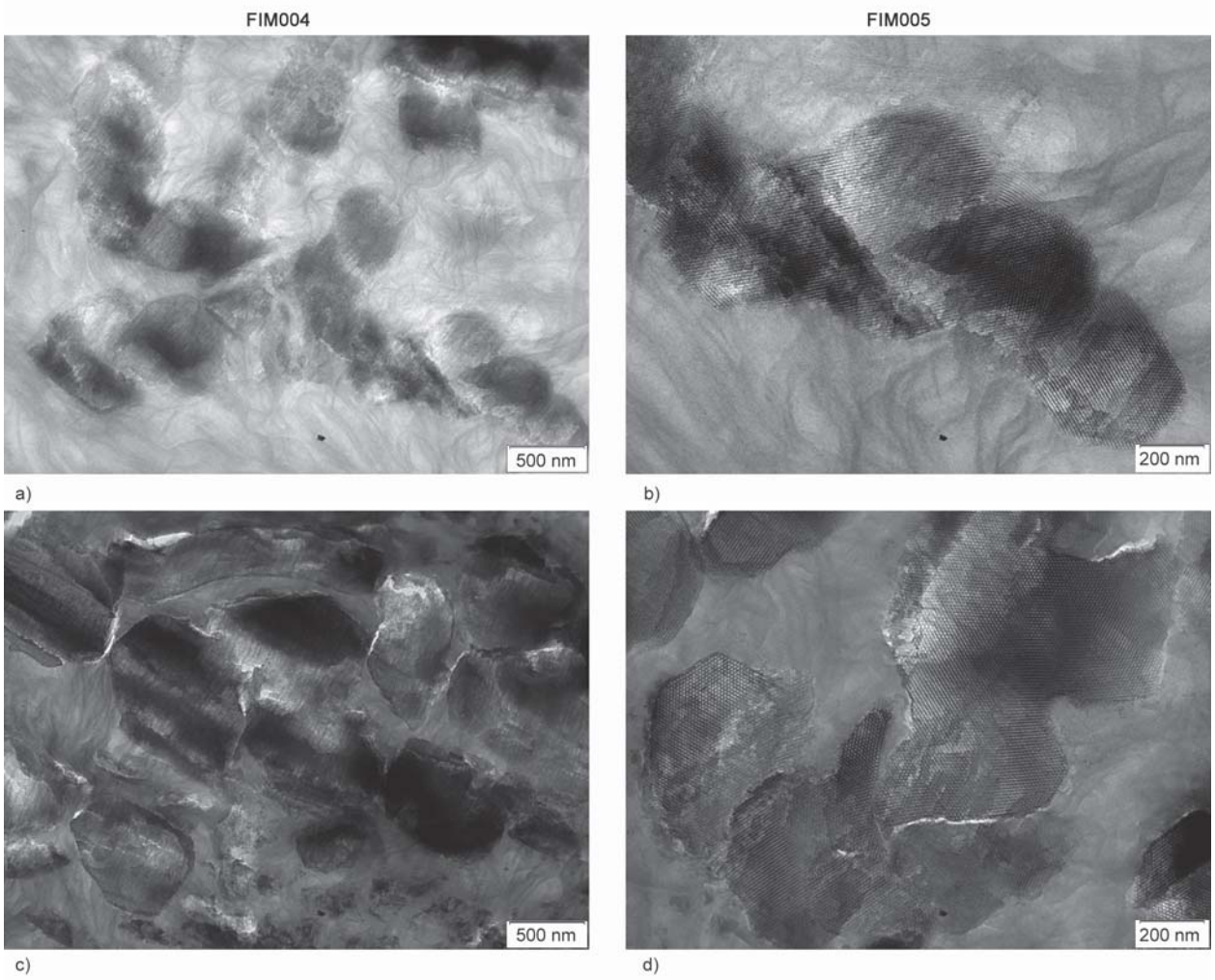

Figure 9. TEM micrographs for the FIM004 (a and c) and FIM005 (b and d) blends

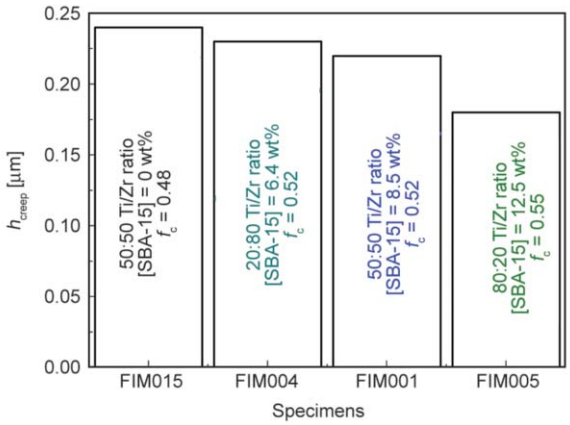

Figure 10. Variation of indentation creep depth for the neat FIM015 blend and blends synthesized by catalysts immobilization on SBA-15 at distinct Ti:Zr ratio and at $Al/M_T = 2500$

crystallinity and the absence of SBA-15 particles are all responsible for its inferior creep resistance. Nevertheless, the FIM005 blend, which follows FIM015 in rigidity features, is the material with the best creep performance at room temperature. This can be due to its highest crystallinity and SBA-15 contents as well as its greater molar mass; all these parameters providing an increased resistance of the macrochains to slippage. The FIM001 and FIM004 samples present similar crystallinity values and intermediate SBA-15 contents. Consequently, creep resistance is lowered when compared with the one in FIM015 in ~5 and 10%, in FIM004 and FM001 blends, respectively, the increasing SBA-15 content being now the key parameter.

3.4. Rheological measurements

To evaluate the rheological behavior of these polymers, several rheological tests were performed on some of the samples. As described in the experimental section, $G(t)$ obtained from step strain experiments was transformed to the frequency space allowing the enlargement of the frequency range up to values as low as $1 \cdot 10^{-4}$ rad/sec.

Figure 11a shows the result from the relaxation experiment for sample FIM001 while Figure 11b exhibits

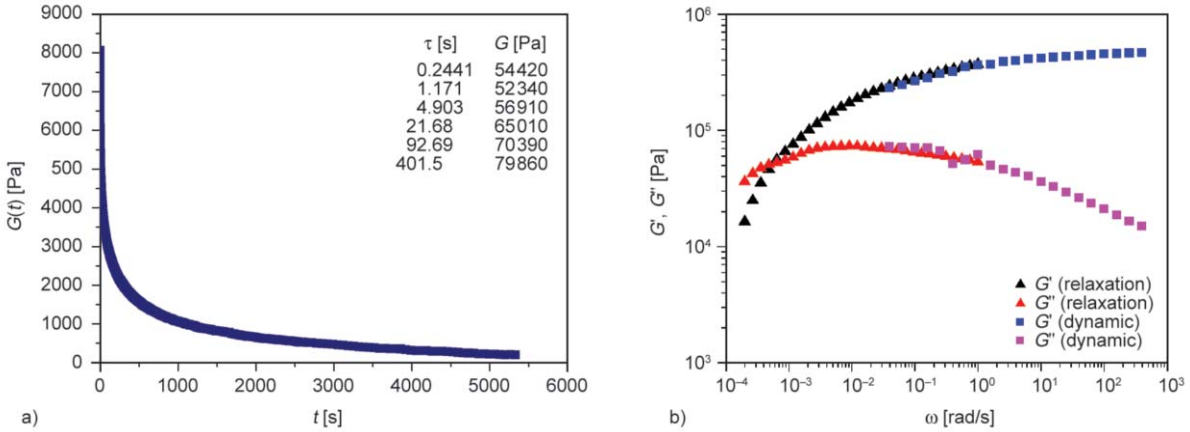

Figure 11. a) $G(t)$ as a function of time from the stress relaxation after a step strain of 2% for sample FIM001, b) Superposition of the stress relaxation (triangles) and dynamic results (squares)

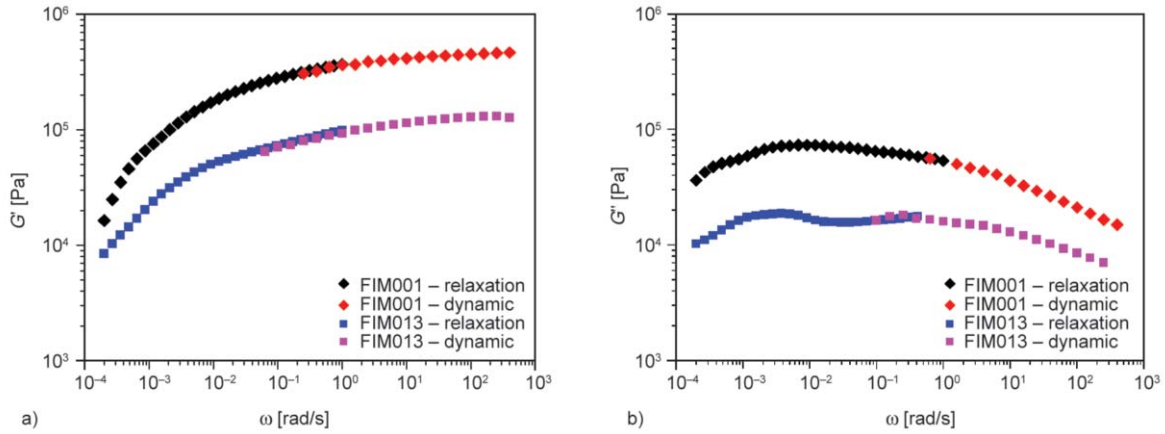

Figure 12. Elastic (a) and loss (b) moduli as a function of frequency for samples FIM013 (squares), FIM001 (diamonds) synthesized under similar conditions but with different SBA-15 content

those from the superposition obtained with the dynamic data after the conversion of the step strain results. An excellent overlap is achieved between both experiments.

The results of the combined experiments for samples FIM001 and FIM013, synthesized under identical polymerization conditions and differing only in the reaction time are shown in Figure 12. Sample FIM013 exhibits lower $G'(\omega)$ values over the whole frequency range covered by both experiments regardless of its higher molar mass, as determined from the SEC measurements. This fact is attributed to the lower SBA-15 content (4.3%) of this sample, versus the 8.5% of SBA-15 in sample FIM001.

The comparison between the samples prepared with different Ti:Zr molar proportions is depicted in Figure 13 by looking at the dependence of $G'(\omega)$ on frequency for samples FIM008, FIM009 and FIM013. The increment in the proportion of the FI catalyst turns out in a polymer with higher molar mass. This feature is reflected in the rheological measurements

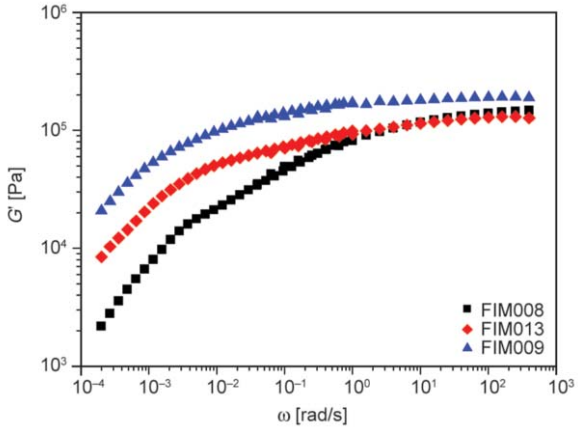

Figure 13. Elastic modulus as a function of frequency for samples FIM008 (squares), FIM013 (diamonds) and FIM009 (triangles) containing 20, 50 and 80% of phenoxi-imine catalyst, respectively

that are in agreement with the results from the SEC. The $G'(\omega)$ for the FIM009 sample exhibits a higher modulus over the whole dynamic range covered by the experiments followed by FIM013, which possesses an intermediate molar mass. The lowest $G'(\omega)$

values are those observed for sample FIM008 with the lowest molar mass.

A common feature of the entirely rheological measurements is the level of the $G'(\omega)$ plateau that is reached for the different samples. In all cases, the modulus of the measured plateau is well below that corresponding to the well-known plateau modulus for polyethylene that is about 1.9 MPa [37]. This is a characteristic result of the rheological data that are obtained from the nascent UHMWPE powder taken just after polymerization [17, 38–42]. This low value is due to the practically absence of entanglements existing in the powder produced during the UHMWPE polymerization at low temperatures. Moreover, the low density of entanglements is, probably, also due to the fact that some polymeric chains are obtained within the confined structure of SBA-15. These conditions favor the obtainment of highly disentangled UHMWPE. Attempts to follow the re-entanglement process by maintaining the polymer samples at 160 °C in the rheometer chamber for long periods of time have been unsuccessful because the polymeric samples degrade acquiring a dark brownish color. The presence of the SBA-15 probably contributes to this process. Rheological studies to follow the re-entanglement kinetics on polybutadienes in solution and in the molten state have demonstrated that the time required for re-entanglement of partially disentangled melts exceeds the terminal relaxation times determined from linear viscoelastic measurements [43, 44] by an order of magnitude. In the particular case of UHMWPE, several works reported by Rastogi and coworkers have demonstrated that periods of time up to several days at temperatures of 160 °C may be required to achieve the complete entangled thermodynamic equilibrium state [38, 41].

4. Conclusions

Several in-reactor UHMWPE/HDPE blends with different compositions have been produced by *in situ* polymerization in a single reactor. The activities and the kinetic profiles obtained during the preparation of these blends can be rationalized taking into account the contribution of each one of the immobilized catalysts. The highest activity is obtained for the blend prepared at a fixed Al/Metal ratio of 2500 and with a Ti:Zr ratio of 50:50. For the blends prepared at a constant Ti:Zr molar proportion the activity increases with the Al/Ti ratio.

The characterization of these blends by TGA under inert atmosphere revealed that decomposition tends to start at higher temperature as the Ti:Zr ratio in the support is increased, *i.e.* as molar mass rises. Under oxidative conditions a more complex behavior is seen. Moreover increasing amounts of SBA-15 in the blends seem to promote degradation.

The DSC traces of the in-reactor blends revealed a single melting and crystallization peak, indicating that the individual chains synthesized by each one of the two catalysts undergo their thermal transitions at identical temperature interval. Moreover the T_m is shifted to slightly higher values as the Ti:Zr ratio increases and a small shoulder appears in the temperature interval ranging from 100 to 125 °C. This may be attributed to polyethylene crystallites, either coming from the UHMWPE or the HDPE component developed inside the SBA-15 channels.

The preliminary evaluation of mechanical response of the distinct polyethylene films has shown that the effect of SBA-15 incorporation in the PE matrix depends on its molar mass. For HDPE samples, issued from zirconocene catalyst, E_{it} does not change significantly with incorporation of SBA-15, however a meaningful increase of H_{it} is observed. On the other hand, a much stronger reinforcement effect of SBA-15 particles, either in bulk rigidity or superficial hardness, is seen in the softer and less crystalline UHMWPE samples. Accordingly, the mechanical behavior of these in-reactor UHMWPE/HDPE blends is complex and depends both on the proportion between these two PE components and the SBA-15 amount. It is also worthwhile noticing that a significant reinforcing effect is seen by adding of a small amount of the UHMWPE component to a HDPE matrix.

Rheological behavior of these blends is dependent on both SBA-15 content and molar masses. In addition, the rheological data obtained from the nascent powders points out that the combination of a multisite catalysts approach with the confined polymerization environment provided by the SBA-15 mesoporous silica support, leads to the formation of a disentangled state in nascent UHMWPE.

Acknowledgements

Financial support of Fundação para a Ciência e Tecnologia, Portugal (SFRH/BD/72761/2010 and UID/QUI/00100/2013), PAUILF (Project TC 07/13), MINECO-Spain (Projects MAT2013-47972-C2-1-P and MAT2013-47972-C2-2-P) and CYTED Red Temática 311RT0417 is acknowledged.

References

[1] Han B., Zhang J., Zhang S., Zhang C.: Study on the processability of UHMWPE filled with different size distribution calcium carbonate particles. Polymer Composites, **36**, 1807–1812 (2015). https://doi.org/10.1002/pc.23087

[2] Shin J., Kim J-C., Chang J-H.: Characterizations of ultrahigh molecular weight polyethylene nanocomposite films with organomica. Polymer Engineering and Science, **51**, 679–686 (2011). https://doi.org/10.1002/pen.21870

[3] Puértolas J., Kurtz S.: Evaluation of carbon nanotubes and graphene as reinforcements for UHMWPE-based composites in arthroplastic applications: A review. Journal of the Mechanical Behavior of Biomedical Materials, **39**, 129–145 (2014). https://doi.org/10.1016/j.jmbbm.2014.06.013

[4] Park H-J., Kwak S-Y., Kwak S.: Wear-resistant ultra high molecular weight polyethylene/zirconia composites prepared by *in situ* Ziegler-Natta polymerization. Macromolecular Chemistry and Physics, **206**, 945–950 (2005). https://doi.org/10.1002/macp.200400350

[5] Tinçer T., Coşkun M.: Melt blending of ultra high molecular weight and high density polyethylene: The effect of mixing rate on thermal, mechanical, and morphological properties. Polymer Engineering and Science, **33**, 1243–1250 (1993). https://doi.org/10.1002/pen.760331904

[6] Diop M., Burghardt W., Torkelson J.: Well-mixed blends of HDPE and ultrahigh molecular weight polyethylene with major improvements in impact strength achieved via solid-state shear pulverization. Polymer, **55**, 4948–4958 (2014). https://doi.org/10.1016/j.polymer.2014.07.050

[7] Soares J. B. P., Kim J. D.: Copolymerization of ethylene and α-olefins with combined metallocene catalysts. I. A formal criterion for molecular weight bimodality. Journal Polymer Science Part A: Polymer Chemistry, **38**, 1408–1416 (2000). https://doi.org/10.1002/(SICI)1099-0518(20000501)38:9<1408::AID-POLA2>3.0.CO;2-8

[8] Kim J. D., Soares J. B. P.: Copolymerization of ethylene and α-olefins with combined metallocene catalysts. III. Production of polyolefins with controlled microstructures. Journal Polymer Science Part A: Polymer Chemistry, **38**, 1427–1432 (2000). https://doi.org/10.1002/(SICI)1099-0518(20000501)38:9<1427::AID-POLA4>3.0.CO;2-Y

[9] Soares J. B. P., Kim J. D., Rempel G. L.: Analysis and control of the molecular weight and chemical composition distributions of polyolefins made with metallocene and Ziegler–Natta catalysts. Industrial and Engineering Chemistry Research, **36**, 1144–1150 (1997). https://doi.org/10.1021/ie960479x

[10] Shan C L. P., Soares J. B. P., Penlidis A.: HDPE/LLDPE reactor blends with bimodal microstructures – Part I: mechanical properties. Polymer, **43**, 7345–7365 (2002). https://doi.org/10.1016/S0032-3861(02)00703-6

[11] Kurek A., Mark S., Enders M., Stürzel M., Mülhaupt R.: Two-site silica supported Fe/Cr catalysts for tailoring bimodal polyethylenes with variable content of UHMWPE. Journal of Molecular Catalysis A: Chemical, **383**, 53–57 (2014). https://doi.org/10.1016/j.molcata.2013.11.020

[12] Kurek A., Xalter R., Stürzel M., Mülhaupt R.: Silica nanofoam (NF) supported single- and dual-site catalysts for ethylene polymerization with morphology control and tailored bimodal molar mass distributions. Macromolecules, **46**, 9197–9201 (2013). https://doi.org/10.1021/ma401971c

[13] Kurek A., Mark S., Enders M., Kristen M., Mülhaupt R.: Mesoporous silica supported multiple single-site catalysts and polyethylene reactor blends with tailor-made trimodal and ultra-broad molecular weight distributions. Macromolecular Rapid Communications, **31**, 1359–1363 (2010). https://doi.org/10.1002/marc.201000074

[14] Stürzel M., Mihan S., Mülhaupt R.: From multisite polymerization catalysis to sustainable materials and all-polyolefin composites. Chemical Reviews, **116**, 1398–1433 (2016) https://doi.org/10.1021/acs.chemrev.5b00310

[15] Rastogi S., Lippits D. R., Peters G. W. M., Graf R., Yao Y., Spiess H. W.: Heterogeneity in polymer melts from melting of polymer crystals. Nature Materials, **4**, 635–641 (2005). https://doi.org/10.1038/nmat1437

[16] Romano D., Ronca S., Rastogi S.: A hemi-metallocene chromium catalyst with trimethylaluminum-free methylaluminoxane for the synthesis of disentangled ultrahigh molecular weight polyethylene. Macromolecular Rapid Communications, **36**, 327–331 (2015). https://doi.org/10.1002/marc.201400514

[17] Pandey A., Champouret Y., Rastogi S.: Heterogeneity in the distribution of entanglement density during polymerization in disentangled ultrahigh molecular weight polyethylene. Macromolecules, **44**, 4952–4960 (2011). https://doi.org/10.1021/ma2003689

[18] Ronca S., Forte G., Tjaden H., Yao Y., Rastogi S.: Tailoring molecular structure *via* nanoparticles for solvent-free processing of ultra-high molecular weight polyethylene composites. Polymer, **53**, 2897–2907 (2012). https://doi.org/10.1016/j.polymer.2012.04.051

[19] Ferreira A. E., Cerrada M. L., Pérez E., Lorenzo V., Cramail H., Lourenço J. P., Ribeiro M. R.: UHMWPE/SBA-15 nanocomposites synthesized by *in situ* polymerization. Microporous and Mesoporous Materials, **232**, 13–25 (2016). https://doi.org/10.1016/j.micromeso.2016.06.002

[20] Campos J. M., Ribeiro M. R., Lourenço J. P., Fernandes A.: Ethylene polymerisation with zirconocene supported in Al-modified MCM-41: Catalytic behaviour and polymer properties. Journal of Molecular Catalysis A: Chemical, **277**, 93–101 (2007). https://doi.org/10.1016/j.molcata.2007.07.026

[21] Quinn F. A., Mandelkern L.: Thermodynamics of crystallization in high polymers: Poly-(ethylene)[1]. Journal of the American Chemical Society, **80**, 3178–3182 (1958). https://doi.org/10.1021/ja01546a003

[22] Oliver W. C., Pharr G. M.: An improved technique for determining hardness and elastic modulus using load and displacement sensing indentation experiments. Journal of Materials Research, **7**, 1564–1583 (1992). https://doi.org/10.1557/JMR.1992.1564

[23] Ferry J. D.: Viscoelastic properties of polymers. Wiley, New York (1980).

[24] Baier M. S., Zuideveld M. A., Mecking S.: Post-metallocenes in the industrial production of polyolefins. Angewandte Chemie International Edition, **53**, 9722–9744 (2014). https://doi.org/10.1002/anie.201400799

[25] Makio H., Terao H., Iwashita A., Fujita T.: FI catalysts for olefin polymerization – A comprehensive treatment. Chemical Reviews, **111**, 2363–2449 (2011). https://doi.org/10.1021/cr100294r

[26] Mitani M., Mohri J-I., Yoshida Y., Saito J., Ishii S., Tsuru K., Matsui S., Furuyama R., Nakano T., Tanaka H., Kojoh S-i., Matsugi T., Kashiwa N., Fujita T.: Living polymerization of ethylene catalyzed by titanium complexes having fluorine-containing phenoxy–imine chelate ligands. Journal of the American Chemical Society, **124**, 3327–3336 (2002). https://doi.org/10.1021/ja0117581

[27] Iwashita A., Chan M. C. W., Makio H., Fujita T.: Attractive interactions in olefin polymerization mediated by post-metallocene catalysts with fluorine-containing ancillary ligands. Catalysis Science and Technology, **4**, 599–610 (2014). https://doi.org/10.1039/c3cy00671a

[28] Sinfrônio F. S. M., Souza A. G., Santos I. M. G., Fernandes Jr. V. J., Novák Cs., Éhen Zs.: Influence of H-ZSM-5, Al-MCM-41 and acid hybrid ZSM-5/MCM-41 on polyethylene decomposition. Journal of Thermal Analysis and Calorimetry, **85**, 391–399 (2006). https://doi.org/10.1007/s10973-006-7535-0

[29] Marcilla A., Gómez-Siurana A., Menargues S., Ruiz-Femenia R., García-Quesada J. C.: Oxidative degradation of EVA copolymers in the presence of MCM-41. Journal of Analytical and Applied Pyrolysis, **76**, 138–143 (2006). https://doi.org/10.1016/j.jaap.2005.10.004

[30] Campos J. M., Lourenço J. P., Pérez E., Cerrada M. L., Ribeiro M. R.: Self-reinforced hybrid polyethylene/MCM-41 nanocomposites: *In-situ* polymerisation and effect of MCM-41 content on rigidity. Journal of Nanoscience and Nanotechnology, **9**, 3966–3974 (2009). https://doi.org/10.1166/jnn.2009.1298

[31] Aguado J., Serrano D. P., Romero M. D., Escola J. M.: Catalytic conversion of polyethylene into fuels over mesoporous MCM-41. Chemical Communications, 725–726 (1996). https://doi.org/10.1039/cc9960000725

[32] Chaianansutcharit S., Katsutath R., Chaisuwan A., Bhaskar T., Nigo A., Muto A., Sakata Y.: Catalytic degradation of polyolefins over hexagonal mesoporous silica: Effect of aluminum addition. Journal of Analytical and Applied Pyrolysis, **80**, 360–368 (2007). https://doi.org/10.1016/j.jaap.2007.04.009

[33] Cerrada M. L., Pérez E., Lourenço J. P., Campos J. M., Ribeiro M. R.: Hybrid HDPE/MCM-41 nanocomposites: crystalline structure and viscoelastic behaviour. Microporous and Mesoporous Materials, **130**, 215–223 (2010). https://doi.org/10.1016/j.micromeso.2009.11.009

[34] Cerrada M. L., Bento A., Pérez E., Lorenzo V., Lourenço J. P., Ribeiro M. R.: Hybrid materials based on polyethylene and MCM-41 microparticles functionalized with silanes: Catalytic aspects of *in situ* polymerization, crystalline features and mechanical properties. Microporous and Mesoporous Materials, **232**, 86–96 (2016). https://doi.org/10.1016/j.micromeso.2016.06.011

[35] Collins M. N., Dalton E., Schaller B., Leahy J. J., Birkinshaw C.: Crystal morphology of strained ultra high molecular weight polyethylenes. Polymer Testing, **31**, 629–637 (2012). https://doi.org/10.1016/j.polymertesting.2012.03.009

[36] Cerrada M. L., Pérez E., Lourenço J. P., Bento A., Ribeiro M. R.: Decorated MCM-41/polyethylene hybrids: crystalline details and viscoelastic behavior. Polymer, **54**, 2611–2620 (2013). https://doi.org/10.1016/j.polymer.2013.03.010

[37] Wood-Adams P. M., Dealy J. M., deGroot A. W., Redwine O. D.: Effect of molecular structure on the linear viscoelastic behavior of polyethylene. Macromolecules, **33**, 7489–7499 (2000). https://doi.org/10.1021/ma991533z

[38] Talebi S., Duchateau R., Rastogi S., Kaschta J., Peters G. W. M., Lemstra P. J.: Molar mass and molecular weight distribution determination of UHMWPE synthesized using a living homogeneous catalyst. Macromolecules, **43**, 2780–2788 (2010). https://doi.org/10.1021/ma902297b

[39] Li W., Guan C., Xu J., Mu J., Gong D., Chen Z-R., Zhou Q.: Disentangled UHMWPE/POSS nanocomposites prepared by ethylene *in situ* polymerization. Polymer, **55**, 1792–1798 (2014). https://doi.org/10.1016/j.polymer.2014.02.023

[40] Gao P., Mackley M. R.: The structure and rheology of molten ultra-high-molecular-mass polyethylene. Polymer, **35**, 5210–5216 (1994). https://doi.org/10.1016/0032-3861(94)90471-5

[41] Romano D., Andablo-Reyes E., Ronca S., Rastogi S.: Aluminoxane co-catalysts for the activation of a bis phenoxyimine titanium (IV) catalyst in the synthesis of disentangled ultra-high molecular weight polyethylene. Polymer, **74**, 76–85 (2015). https://doi.org/10.1016/j.polymer.2015.07.039

[42] Li N., Zhang Q., Yang Q., Huang Y., Liao X., Zhao W.: The dependence time of melting behavior on rheological aspects of disentangled polymer melt: A route to the heterogeneous melt. Journal of Polymer Research, **22**, 1–7 (2015). https://doi.org/10.1007/s10965-015-0681-y

[43] Robertson C. G., Warren S., Plazek D. J., Roland C. M.: Reentanglement kinetics in sheared polybutadiene solutions. Macromolecules, **37**, 10018–10022 (2004). https://doi.org/10.1021/ma048148g

[44] Roy D., Roland C. M.: Reentanglement kinetics in polyisobutylene. Macromolecules, **46**, 9403–9408 (2013). https://doi.org/10.1021/ma402074b